Probing the adsorption of nonionic micelles on different-sized nanoparticles by scattering techniques

Himanshi Singh,[1,2] Debes Ray,[1] Sugam Kumar,[1] Shin-ichi Takata,[3] Vinod K. Aswal,[1,2,*] and Hideki Seto[4]

[1]*Solid State Physics Division, Bhabha Atomic Research Centre, Mumbai 400 085, India*

[2]*Homi Bhabha National Institute, Mumbai 400 094, India*

[3]*J-PARC Center, Japan Atomic Energy Agency, Tokai, Ibaraki 319-1195, Japan*

[4]*J-PARC Center, High Energy Accelerator Research Organization, Tokai, Ibaraki 319-1106, Japan*

(Received 1 September 2020; revised 28 October 2020; accepted 11 November 2020; published 1 December 2020)

The interaction of nanoparticles with surfactants is extensively used in a wide range of applications from enhancing colloidal stability to phase separation processes as well as in the synthesis of noble functional materials. The interaction is highly specific depending on the charged nature of the surfactant. In the case of nonionic surfactants, the micelles adsorb on the surface of nanoparticles. The adsorption of nonionic surfactant C12E10 as a function of surfactant concentration for two different sizes of anionic silica nanoparticles (16 and 27 nm) has been examined using dynamic light scattering (DLS) and small-angle neutron scattering (SANS). SANS measurements have been carried out under different contrast-matched conditions, where nanoparticles, as well as surfactant micelles, have been contrast-matched to the solvent. The adsorption of micelles is determined from the contrast-matched condition of silica nanoparticles with the solvent. SANS data under surfactant contrast-matched condition suggest that there is no modification in the structure and/or interaction of the silica nanoparticles in presence of nonionic micelles. The adsorption of micelles on nanoparticles is found to follow an exponential behavior with respect to the surfactant concentration. These results are consistent with the variation of hydrodynamic size of nanoparticle-surfactant system in DLS. The study on different-sized nanoparticles shows that the lower curvature enhances the packing fraction whereas the loss of surface-to-volume ratio suppresses the fraction of adsorbed micelles with the increase in the nanoparticle size. The adsorption coefficient has higher value for the larger size of the nanoparticles. In the mixed system of two sizes of nanoparticles, no preferential selectivity of micelle adsorption is observed.

DOI: 10.1103/PhysRevE.102.062601

I. INTRODUCTION

The emerging applications of nanoparticle-macromolecule complexes influence great scientific attention to the field of nanoscience and nanotechnology. Various macromolecules such as proteins, surfactants, and polymers when conjugated with nanoparticles exhibit the formation of unique functional materials. The modeling of potent nanoparticle-macromolecule conjugates finds numerous applications such as the production of multifunctional materials, extended spread time, the solubility of drugs, catalysis, enhancing the performance of surface-active agents, in biomedicine and therapeutics, to name a few [1–7].

One of the most important aspects of these hybrid soft matter systems is the underlying interactions such as van der Waals force, electrostatic interaction, hydrogen bonding, etc., which are governed by various characteristic features of individual nanoparticles as well as macromolecule [8–13]. The inclusion of macromolecules in nanoparticle solution, therefore, results in significant changes in the phase behavior and the resultant structure. One of the most prominent macromolecules is surfactant molecules which are amphiphilic in nature, consisting of hydrophilic head groups and hydrophobic tails. Depending upon the charge possessed by their head group, they are further categorized as nonionic, anionic, cationic, or zwitterionic. Upon dispersion in an aqueous medium, these surfactant molecules form self-assembled structures, known as micelles, primarily due to the simultaneous presence of hydrophobic and hydrophilic entities inside a single molecule [14–16]. The surfactants arrange themselves such that the hydrophobic part forms the inner core of the micelles while the hydrophilic part faces solvent [17,18]. There are significant differences observed in the interactive behavior between nanoparticle and surfactant depending on the polarity of the surfactant [19,20]. In the case of similar charged surfactant to the nanoparticles (e.g., anionic surfactant and anionic nanoparticles), the surfactant micelles coexist with nanoparticles without any physical interaction because of the charge repulsion between them. On the other hand, oppositely charged surfactant micelles strongly adsorb on the nanoparticles and lead to their aggregation. The nonionic surfactant micelles have been found to show the phenomenon of adsorption resulting in the micelle-decorated nanoparticle surface. The formation of hydrogen bonds between the ether head groups of the surfactant and the surface silanol (Si-OH) groups of silica is behind the formation of this core-shell structure [21–23]. The adsorption of nonionic surfactant micelles strongly depends on various parameters such as temperature, concentration, and molecular structure of the surfactant [24–27].

In this work, the evolution of adsorption of nonionic surfactant micelles on charge-stabilized silica nanoparticles as a function of surfactant concentration has been studied.

*vkaswal@barc.gov.in

Also, a strong emphasis has been given on understanding the effect of different sized nanoparticles on the adsorption behavior and their selectivity for mixed sizes of nanoparticles. It has been achieved in a system of nonionic surfactant decaethylene glycol monododecylether (C12E10) and anionic silica nanoparticles (Ludox HS40 and TM40) in aqueous solution. All the measurements were carried out for a fixed concentration (1 wt %) of silica nanoparticles and varying the concentration of surfactant in the range of 0–1 wt %. The adsorption of C12E10 micelles on the surface of silica nanoparticles has been found to show exponential growth behavior in the entire surfactant concentration regime, irrespective of the size of the nanoparticles. However, the curvature of nanoparticles and available surface area for the adsorbents decides the efficiency of adsorption which is markedly different for the two sizes. In the mixed system of these differently sized nanoparticles, it has been looked into whether the micelles show any kind of preferential selectivity for particular nanoparticle size in the adsorption. Scattering techniques such as small-angle neutron scattering (SANS) and dynamic light scattering (DLS) have been employed to investigate the nanoparticle-surfactant conjugate systems. The structural details of the individual constituents in the conjugates have been investigated by utilizing the contrast-matching technique of SANS. The surface-modified nanoparticles due to the presence of surfactant micelles have significant implications in terms of colloidal stability and interfacial behavior [5,28–30]. A scientific understanding of adsorption resulting in the conjugated structures is necessary to optimize the performance of nanoparticles-surfactant composites at applied levels.

II. EXPERIMENT

A. Materials

Electrostatically stabilized 40 wt % colloidal suspensions of silica nanoparticles (Ludox HS40 and TM40) and nonionic surfactant C12E10 were purchased from Sigma-Aldrich. Distilled deionized water from Millipore MilliQ unit and 99.9% pure D_2O were used for the sample preparation. Samples were prepared by dissolving a weighted amount of silica nanoparticle(s) (1 wt %) and surfactant (0 to 1 wt %) in an appropriate solvent. Distilled deionized water was used to make samples in DLS whereas D_2O and mixed D_2O/H_2O were used as solvents for SANS and contrast-matching SANS, respectively. In contrast-matched SANS experiments, the solvents H_2O and D_2O provide different contrasts for the constituents because of very different neutron scattering lengths for H and D. The calculated neutron scattering length densities of H_2O, D_2O, C12E10, and silica nanoparticles are -0.56×10^{10}, 6.38×10^{10}, 0.30×10^{10}, and 3.81×10^{10} cm^{-2}, respectively.

B. Methods

Small-angle neutron scattering experiments were performed at the Small and Wide Angle Neutron Scattering Instrument (TAIKAN) at J-PARC, Japan [31]. It is a time-of-flight small-angle neutron scattering instrument making use of pulsed neutrons in a wide wavelength range. The wavelength range used in the measurements was 0.8–7.6 Å. The scattered neutrons were detected by using three detector banks of small, middle, and high angle to cover the data in the wide scattering vector Q range ($Q = 4\pi \sin\theta/\lambda$, where λ is the wavelength of the incident neutrons and 2θ is the scattering angle). Freshly prepared samples were held in quartz cells having thicknesses of 1 and 2 mm, and the temperature was kept constant at 25 °C during the measurements. The data were corrected and normalized at absolute scale using a standard procedure. The nanoparticle-surfactant systems were studied with the three contrast conditions: (i) no contrast-matching (in 100 vol % D_2O), (ii) surfactant micelles are contrast-matched (in 13 vol % D_2O), and (iii) silica nanoparticles are contrast-matched (in 62 vol % D_2O). A multicomponent system can be simplified to study its constituents by selectively contrast-matching that particular constituent with the solvent. The fact that the scattering length densities of H_2O and D_2O are very different from each other and the contrast-matched point is obtained by mixing them in a ratio where scattering length density of H_2O/D_2O mixed solvent matches with the particular component to be contrast-matched. The contrast-matched point of silica nanoparticles is around 62 vol % of D_2O whereas in the case of C12E10 micelles it is around 13 vol % D_2O in the D_2O/H_2O mixed solvent [21–23,32].

Dynamic light scattering measurements were carried out using a SZ-100 particle size analyzer (Horiba, Japan) at a back-scattering angle 173° and a fixed wavelength of 532 nm.

C. Small-angle neutron scattering analysis

In SANS measurement, the differential scattering cross section per unit volume ($d\Sigma/d\Omega$) as a function of wave vector transfer Q is measured. In the case of a system of monodisperse spherical particles in a medium, it is expressed as [33,34]

$$\left(\frac{d\Sigma}{d\Omega}\right)(Q) = nP(Q)S(Q) + B, \tag{1}$$

where n denotes the number density of particles. $P(Q)$ is the intraparticle structure factor and $S(Q)$ is the interparticle structure factor. B is a constant term representing incoherent background scattering, which is mainly due to the hydrogen present in the sample.

Intraparticle structure factor $P(Q)$ is decided by the shape and the size of the particle and is the square of form factor amplitude $F(Q)$ as determined by

$$P(Q) = V^2(\rho_p - \rho_s)^2\langle|F(Q)|^2\rangle, \tag{2}$$

where V is the volume of the particle, and ρ_p and ρ_s are the scattering length densities of particle and solvent, respectively.

For a spherical particle of radius R, $F(Q)$ is given by [35]

$$F(Q) = 3\left[\frac{\sin(QR) - QR\cos(QR)}{(QR)^3}\right]. \tag{3}$$

In the case of core-shell structure having core radius R_c and thickness t, $P(Q)$ can be written as [35]

$$P(Q) = \left[(\rho_c - \rho_{\text{shell}}) V_c \left\{ \frac{3 j_1(QR_c)}{QR_c} \right\} + (\rho_{\text{shell}} - \rho_s) V_m \left\{ \frac{3 j_1(QR_m)}{QR_m} \right\} \right]^2, \quad (4)$$

where ρ_c, ρ_{shell}, and ρ_s are, respectively, the neutron scattering length densities of the core, shell, and solvent. $V_c = (4\pi/3)Rc^3$ and $V_m = (4\pi/3){R_m}^3 (R_m = R_c + t)$ are volumes of core and core along with shell, respectively.

$S(Q)$ describes the interaction between the particles present in the system and it is the Fourier transform of the pair correlation function for the mass centers of the particles. For dilute systems, $S(Q) \sim 1$. In the case of an interacting isotropic system, $S(Q)$ can be written as

$$S(Q) = 1 + 4\pi n \int [g(r) - 1] \frac{\sin Qr}{Qr} r^2 dr, \quad (5)$$

where $g(r)$ is the radial distribution function. It is the probability of finding the particle at a distance r from a reference particle centered at the origin. The $g(r)$ is governed by the form of the potential $V(r)$.

In the case of interaction leading to the adsorption or decoration of micelles on the nanoparticles, the scattering cross section comprises four terms: two terms correspond to the scattering from nanoparticles and micelles, the third term is a cross term between the adsorbed micelles and the nanoparticles, and the last term represents the cross term between different adsorbed micelles on the nanoparticle surface [36]. The contributions from the nanoparticle and the interference term between the nanoparticle and micelles cancel out when the nanoparticles are contrast-matched to the solvent. The scattering from the remaining two terms (micelles and the micelle-micelle interference) can be simplified as

$$\left(\frac{d\Sigma}{d\Omega} \right)(Q) = n_m P_m(Q) S_{mm}(Q) + B, \quad (6)$$

where $P_m(Q)$ is the intraparticle structure factor of the micelles [37,38]. $S_{mm}(Q)$ is the interparticle structure factor and is numerically calculated as

$$S_{mm}(Q) = 1 + \frac{1}{N} \sum_{i=1}^{N} \sum_{j>i}^{N} \frac{\sin\{Q(r_i - r_j)\}}{Q(r_i - r_j)}, \quad (7)$$

where $(r_i - r_j)$ is the distance between the centers of the two micelles adsorbed on the same nanoparticle and N is the number of micelles adsorbed on the nanoparticle surface [38,39].

The data have been analyzed by comparing the scattering from different models to the experimental data. The silica nanoparticles have been fitted with a model of polydispersed spherical particles where radius and polydispersity are the fitted parameters. The parameters for micelles of nonionic surfactant C12E10 have been calculated using a model consisting of a spherical hydrophobic core surrounded by a hydrophilic shell. Micelle-decorated nanoparticles under nanoparticle contrast-matched condition have been modeled as a combination of the scattering from micelles and the interaction between different adsorbed micelles on the nanoparticle surface. Scattering length densities of the scatterers (nanoparticles, micelles) and the solvent are kept fixed. The dimensions of the nanoparticles and micelles as obtained from the analysis of pure nanoparticles and micelles solutions are also kept fixed while carrying out analysis of micelles adsorption on nanoparticles. The number of adsorbed micelles per nanoparticle is used as the only fitting parameter. All the data are fitted using SASFIT analysis software and the data analysis is carried out on an absolute scale [40]. The model scattering is convoluted with the resolution function [31] to compare with the experimental data. The fitted parameters in the analysis were optimized using the nonlinear least-square fitting program to the model scattering [35,41].

D. Dynamic light scattering

The dynamic light scattering measures the temporal fluctuation in scattering light intensity at a specific angle using a monochromatic light. The signal generated by diffusing particles can be analyzed by the normalized intensity autocorrelation function $g^2(\tau)$ [42,43],

$$g^2(\tau) = \frac{\langle I(t) I(t+\tau) \rangle}{\langle I(t) \rangle^2}, \quad (8)$$

where $I(t)$ is the scattered light intensity at time t and $I(t + \tau)$ the scattered intensity at time t plus delay time τ. The normalized intensity correlation function is related to the normalized field autocorrelation function by the Siegert relation,

$$g^2(\tau) = 1 + \beta |g^1(\tau)|^2, \quad (9)$$

where β $(0 < \beta < 1)$ is the spatial coherence factor and depends on the instrument optics. In the case of a monodisperse system of particles, $g^1(\tau)$ decays exponentially and for a polydisperse system it can be written as

$$g^1(\tau) = \int_0^\infty F(\Gamma) \exp(-\Gamma\tau) d\Gamma, \quad (10)$$

where $\Gamma(= DQ^2)$ is the decay constant for a given size, which depends on the diffusion coefficient (D) of the particles and the magnitude of wave vector transfer (Q). $F(\Gamma)$ is the weight factor in the decay constant distribution representing the particle distribution with different diffusion coefficients relative to the mean value.

For a narrow monomodal distribution, the cumulant analysis yields the mean value of diffusion coefficient (D_{m}) and polydispersity index (PI) according to the following equation:

$$g^1(\tau) = \exp\left[-D_m Q^2 \tau + \frac{\mu_2 \tau^2}{2} \right] \quad (11)$$

where μ_2 is the variance. The PI is calculated by the ratio of variance (μ_2) to the square of mean of the decay constant $(\Gamma_m = D_m Q^2)$ [44]. The Stokes-Einstein relation then correlates the hydrodynamic size (diameter) of particles to the diffusion coefficient [45],

$$d_h = \frac{k_B T}{3\pi\eta D_m}, \quad (12)$$

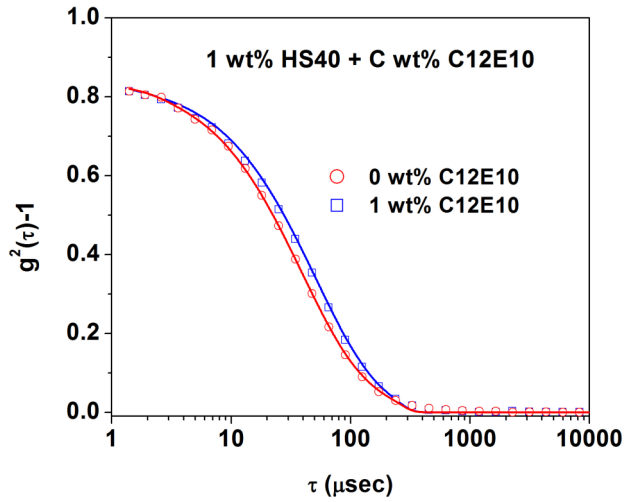

FIG. 1. Plots of DLS autocorrelation functions of 1 wt % HS40 silica nanoparticles in the absence and the presence of 1 wt % C12E10 micelles.

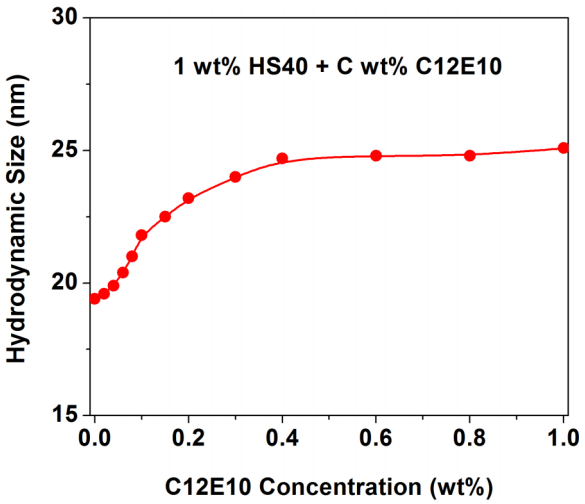

FIG. 2. The variation of mean hydrodynamic size in 1 wt % HS40 silica nanoparticles as a function of C12E10 surfactant concentration (0–1 wt %).

where k_B is Boltzmann's constant, η is the viscosity of the solvent, and T is the absolute temperature. The hydrodynamic size could be very different from the actual size depending on hydration and/or interaction between the particles.

III. RESULTS AND DISCUSSION

Figure 1 shows the DLS data of 1 wt % HS40 silica nanoparticles as well as in the presence of 1 wt % C12E10 micelles. It is observed that the intensity autocorrelation function becomes significantly broader with the addition of 1 wt % C12E10. The effective particle hydrodynamic size has been found to increase from 19.5 nm (only nanoparticles) to 25 nm for the HS40-C12E10 mixed system. The size of the micelles (∼5 nm), being quite small compared to that of the nanoparticles (19.5 nm), and the enhancement in the effective particle hydrodynamic size in the mixed system negates the possibility of coexistence of nanoparticles and micelles in the solution but clearly indicates an interaction between them. This increase in the mean hydrodynamic size can attribute to the possibility of adsorption of C12E10 micelles onto the surface of nanoparticles to form a conjugate structure. The measurement of free micelles from DLS along with nanoparticles is difficult because the signal is dominated by the silica nanoparticles having a much larger size and larger contrast than micelles. The inverse Laplace transform of weighted DLS data does not show the presence of free micelles. It is known that the viscosity of a system has a crucial role to play in determining the effective hydrodynamic size in DLS [Eq. (12)]. Hence, it is important to cross-check whether there is any significant change in the viscosity of the nanoparticle system due to the addition of nonionic micelles, which if not considered could affect the calculation of the hydrodynamic size obtained for the HS40-C12E10 mixed system. For the addition of 1 wt % C12E10 to 1 wt % HS40 solution, the change in the viscosity is very small (∼1%), and the correction for viscosity (without and with C12E10) in the modified hydrodynamic size is negligible. Further, to understand the adsorption behavior of C12E10 micelles on the surface of silica nanoparticles, the measurements have been carried out with the addition of varying concentration of C12E10 into the silica nanoparticle system.

Figure 2 shows the variation of the mean hydrodynamic size in 1 wt % of HS40 silica nanoparticles mixed with varying concentration (0–1 wt %) of C12E10 with an increment of 0.1 wt %. Initially, with the increase in the C12E10 concentration in the solution there is a rise in the mean hydrodynamic size. This may indicate the growing number of adsorbed micelles sitting on the surface of nanoparticles in the initial concentration phase. Beyond a particular C12E10 concentration (∼0.4 wt %), the mean hydrodynamic size shows saturation with a further increase in the surfactant concentration. At this concentration, it may be assumed that a sufficient number of C12E10 micelles have been adsorbed on the surface of the nanoparticles. The saturation contains important information about the effective coverage of the available nanoparticle surface through adsorption and formation of a core-shell-like structure. To study these microstructures directly, contrast-matched SANS experiments have been performed where the multicomponent conjugates are simplified to highlight each of the components separately.

Figures 3(b)–3(d) show the SANS data of the HS40-C12E10 system under three different contrast conditions, in D_2O, 13 vol % D_2O (contrast-match point of C12E10) and 62 vol % D_2O (contrast-match point of silica nanoparticles), respectively. Data analysis of HS40 silica nanoparticles (in D_2O) using a polydispersed spherical particle model gives the mean size of the spherical nanoparticles as 16 nm with polydispersity of 0.15 [Fig. 3(a)]. The size difference in DLS (18 nm) and SANS (16 nm) can be expected from hydration and/or interaction between the particles. SANS is more reliable because the structure and interaction can be separated and the actual size of the particles is determined. SANS data of C12E10 in Fig. 3(a) micelles have been analyzed using a core-shell model consisting of a spherical hydrophobic core surrounded by hydrophilic shell [36]. The mean core size

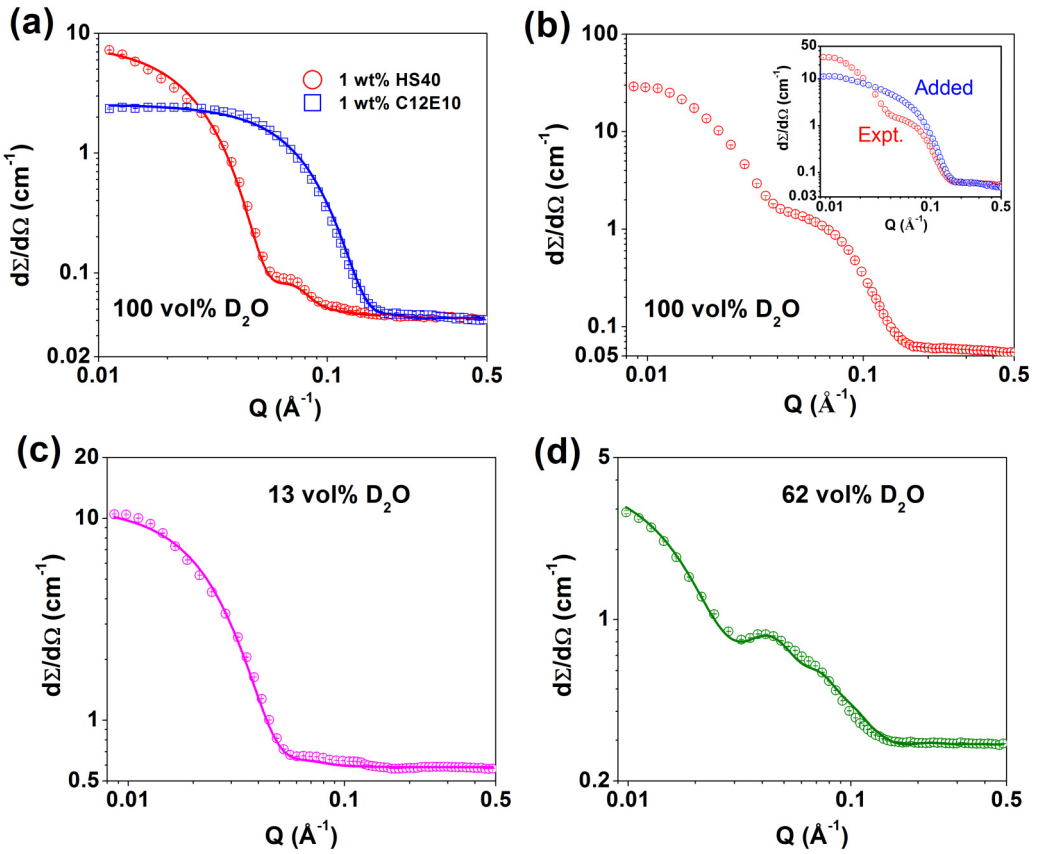

FIG. 3. SANS data of 1 wt % HS40 with 1 wt % C12E10 under different contrast conditions: (a) pure components in D_2O, (b) no component is contrast-matched (100 vol % D_2O) (dissimilarity between the measured data and calculated addition of data is shown in the inset), (c) surfactant micelles are contrast-matched (13 vol % D_2O), and (d) silica nanoparticles are contrast-matched (62 vol % D_2O).

($2R_c$) and the shell thickness (t) of the micelles are found to be 4 and 1.2 nm, respectively. In Fig. 3(b), the SANS data for the mixed system of HS40-C12E10 has the scattering contributions from both the components (nanoparticles as well as surfactant micelles) but the scattering is not simply additive [inset of Fig. 3(b)], confirming the formation of a conjugated structure. This supports the observations made in the DLS data (Fig. 1). Now, to simplify the structure of this multicomponent conjugated structure, contrast-matched SANS measurements have been used. The measurements were done at 13 vol % D_2O where the scattering from C12E10 micelles diminishes, and as a result of that only HS40 nanoparticles are visible to neutrons and contribute to the scattering cross section. In this case, the data in Fig. 3(c) fit to the scattering from individual dilute nanoparticles (parameters as obtained from the nanoparticles in D_2O), suggesting there is no significant change in the structure and/or interaction of the nanoparticles in the presence of micelles. On the other hand, information about the changes in the micelle structure in the presence of nanoparticles is established from the data measured in 62 vol % D_2O where nanoparticles are contrast-matched as shown in Fig. 3(d). The nanoparticle contrast-matched data of the mixed system shows a buildup in scattering in the low-Q region and also, a hump on the mid-Q region (at $Q \sim 0.04\,\text{Å}^{-1}$) which is not seen in the scattering profile of the pure surfactant system. These SANS data are modeled on the basis of the micelle-decorated bead model [20–23,46–52].

The model accounts for the structure of the adsorbed surface micelles on spherical silica nanoparticles in the nanoparticles contrast-matched scenario. The adsorbate-adsorbate structure factor [Eq. (7)] is calculated numerically by considering the random adsorption of the spherical micelles on nanoparticles. In the simulations, a particle of radius R (equal to the mean radius of the nanoparticle) is considered and the spherical micelles are distributed over this particle, where the position of the micelles is allocated randomly in a spherical polar coordinate (r, θ, φ) system, centered at the center of the nanoparticle. The r coordinate is fixed equal to the center-to-center distance (d_{cc}) between micelle and nanoparticle, and θ, φ are randomly chosen. The possibility of adsorption is realized by setting the condition $r = R + R_m$, where R_m is the radius of the adsorbed micelle. The value R_m is taken as the sum of core radius and shell thickness ($R_m = R_c + t$) of the micelles. The placement of the micelles on the nanoparticle surface is carried out one after the other. The overlapping of the micelles is realized by simultaneously calculating the distance (d_{im}) from the center of the new micelle (say n th micelles) to the centers of all the micelles already adsorbed [1 to $(n-1)$th micelle]. The same is then avoided by putting the condition $d_{\text{im}} \geqslant 2R_{\text{m}}$ and immediately placing the next micelle at some other random position [37,53]. The analysis of the data confirms the formation of a core-shell structure where the C12E10 micelles get adsorbed (shell) on the surface of HS40 nanoparticles (core) coexisting with some free micelles.

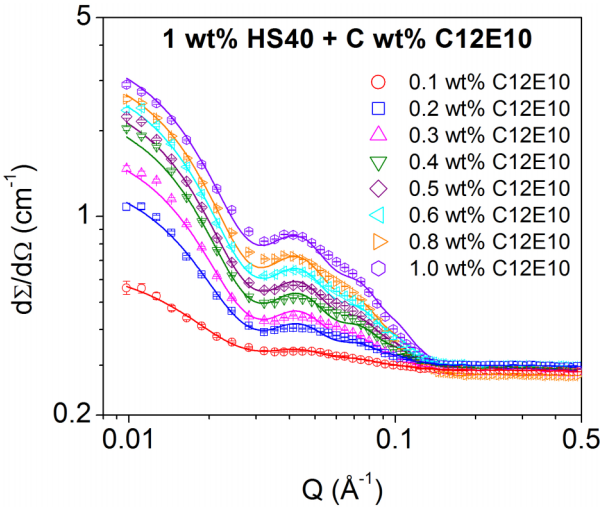

FIG. 4. SANS profiles of 1 wt % HS40 nanoparticles with varying C12E10 surfactant concentration (0.1 to 1 wt %) under nanoparticles contrast-matched condition.

The increase in the mean hydrodynamic size for this mixed system as evidenced in the DLS data is now relatable due to the formation of these micellar-decorated nanostructures. The analysis shows that the number of micelles adsorbed on each nanoparticle is around 15 and about 44% of the total micelles at 1 wt % C12E10 get adsorbed. This adsorption has been attributed to the formation of the hydrogen bonding between the hydrophilic region of surfactant and surface silanol groups (SiOH) of silica nanoparticles [23,48]. We have also looked into the evolution of adsorption of C12E10 micelles on the surface of silica nanoparticles through the addition of varying concentration of C12E10 into the silica nanoparticle system.

The SANS data of 1 wt-% silica nanoparticles with varying concentration of C12E10 when nanoparticles are contrast-matched are shown in Fig. 4. The scattering in the low- and mid-Q region shows significant buildup with an increase in the surfactant concentration from 0.1 to 1 wt %. This enhancement in scattering in the low-Q region is definitely attributed to more and more surfactant micelles introduced in each step of an increase in concentration (when nanoparticles are not contributing to the scattering). The enhancement in the buildup in the mid-Q range arises because of an increase in overall surfactant concentration. Analysis shows that the number of adsorbed micelles per nanoparticle increases when C12E10 concentration increases along with free micelles in the solution. In the lower surfactant concentration regime, at the lower-Q region, the scattering profile shows sharp distinctiveness with the formation of the corona, while at higher concentrations the profiles are almost parallel because of the saturation of micelles in corona. It means that at higher surfactant concentrations, the fraction of free micelles tends to increase. Figure 5(a) shows the fitted structure factor of adsorbed micelles with varying concentration of C12E10. The structure factor contribution solely arises from the excluded volume effect between the micelles. The functionality of structure factor depends on both the sizes of nanoparticles and micelles. For a given size of nanoparticles, the value of structure factor of adsorbed micelles in the low-Q region and structure factor peaks is enhanced without any change in the peak position on increasing the number of adsorbed micelles. The variation of adsorption of micelles on the nanoparticles is shown in the adsorption curve in Fig. 5(b). There is saturation of adsorbed micelles on nanoparticles around 0.5 wt % and the maximum number of adsorbed micelles is 15. These observations are corroborated by the DLS data (Fig. 2) where a similar feature has been noticed for the mean hydrodynamic size with increasing surfactant concentration.

In general, adsorption between adsorbents and adsorbates may involve chemical forces (covalent or coordinate bonding), hydrogen bonding force, electrostatic force, hydrophobic association force, or molecular force. In the present case, it is physisorption (molecular adsorption at the interface) by hydrogen bonding between nanoparticles (adsorbent) and surfactant micelles (adsorbate) [21–23]. The micelle adsorption as a function of surfactant concentration (C) is modeled by $N = N_S(1 - \exp^{-kC})$, where N_S is the saturation value and k is the adsorption coefficient [54,55]. In the initial stage of the adsorption, when the surfactant concentration is well below critical micelle concentration (CMC) (0.01 wt % for C12E10), the surfactant monomers get adsorbed on the nanoparticle surface by orienting themselves conversely, dangling their hydrocarbon chains towards the solution. In this situation (below CMC), the surfactant is adsorbing on a surface where there are very few molecules and the adsorbate-adsorbate interaction

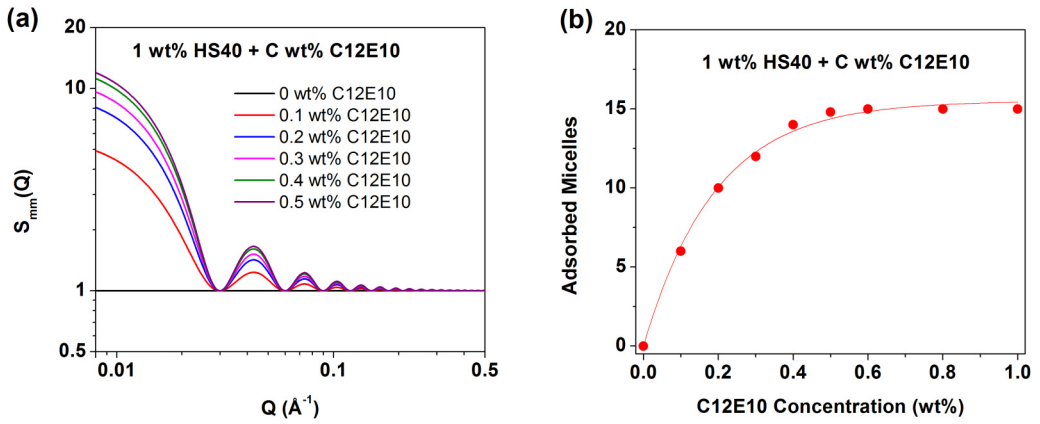

FIG. 5. (a) Structure factor of adsorbed micelles and (b) adsorption curve for C12E10 micelles interacting with HS40 silica nanoparticles.

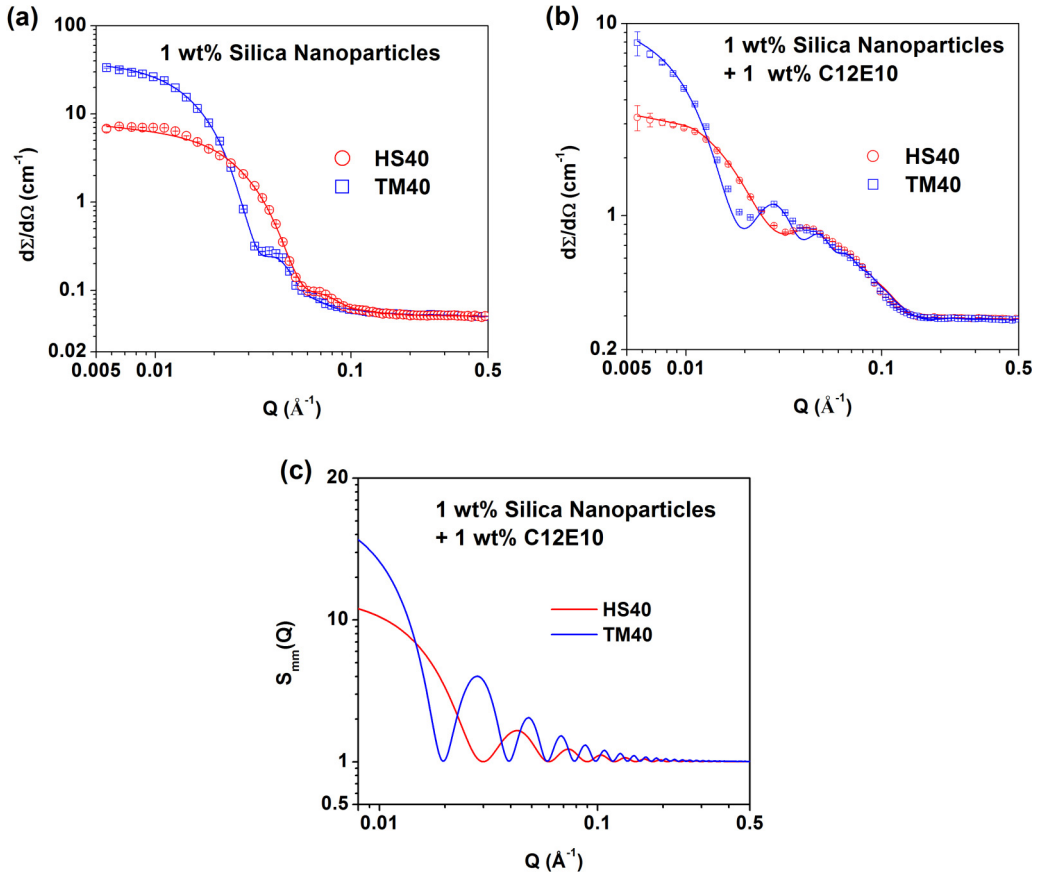

FIG. 6. Comparison of SANS profiles for (a) pure nanoparticles 1 wt % HS40 and 1 wt % TM40 in D_2O and (b) 1 wt % HS40 and 1 wt % TM40 with 1 wt % C12E10 under nanoparticles contrast-matched condition. Panel (c) shows the comparison of structure factor of adsorbed micelles on HS40 and TM40 nanoparticles.

is negligible as the molecules are far away from each other. With the introduction of more and more number of surfactant molecule (just above CMC), local monolayers (hemimicelles) start forming and the slope of the adsorption curve [Fig. 5(b)] starts rising. The monolayer adsorption produces a hydrophobic surface, which eventually forms local bilayers (micelles), and the slope of the adsorption curve proceeds towards saturation. With further increasing surfactant concentration (beyond 0.5 wt %), the excess micelles coexist as free with the adsorbed micelles [27,56]. The average limit of the maximum number of adsorbed micelles on each nanoparticle decides the plateau of the adsorption curve. The hydrodynamic size in Fig. 2 is fitted with the same value of k as obtained from SANS data and using relation $d_h = d_{h0} + d_{hS}(1 - \exp^{-kC})$, where d_{h0} is the hydrodynamic size without surfactant and d_{hS} is the saturation value of hydrodynamic size at higher surfactant concentration.

There are several factors like molecular structure of surfactant, temperature, or electrolyte having an influence on the adsorption and the adsorption curve. This is due to adsorbate-adsorbate and adsorbate-solvent interactions, which cause surfactant aggregation in bulk solution and leads to a change in orientation and packing of surfactants at the surface. For example, within a homologous series it is found that the increasing length of the hydrocarbon chain of nonionic surfactant, increasing temperature and electrolytes, generally increases the magnitude of adsorption at the plateau [27,57,58]. The packing fraction of micelles on the nanoparticle surface and the fraction of adsorbed micelles is expected to strongly depend on the size of the nanoparticles in terms of curvature and available surface area. We have therefore also examined the adsorption behavior of micelles for different sized nanoparticles.

Figure 6(a) shows the SANS data for comparison of 1 wt % of silica nanoparticles HS40 with TM40. Both the nanoparticles show a monotonically decreasing scattering cross section as a function of Q as the scattering is primarily governed by the intraparticle structure factor $P(Q)$. It is known that the scattering profile becomes narrower with an increasing particle size as its width depends inversely on the particle size. The overall scattering intensity also increases with the increasing particle size (proportional to the particle volume at a constant volume fraction of particles). The higher scattering cross section for TM40 compared to that for HS40 and the width variation opposite to this trend indicates the order of increasing particle size for TM40 as compared to HS40. The analysis shows that the silica nanoparticles HS40 and TM40 have mean particle sizes 16 and 27 nm, respectively with a polydispersity of ∼0.15. Now, coming to the conjugate system, Fig. 6(b) shows the SANS data of 1 wt % HS40 and 1 wt % TM40 with 1 wt % C12E10 when nanoparticles are contrast-matched to the solvent (62 vol % of D_2O in H_2O/D_2O). The scattering

TABLE I. Fitted parameters from the SANS data of 1 wt % C12E10 micelles with 1 wt % silica nanoparticles of two different sizes (HS40 and TM40).

Nanoparticle system	Mean size (nm)	Number density (cm^{-3})	Curvature (nm^{-1})	Surface area (nm^2)	Surface to volume ratio (nm^{-1})	Maximum adsorbed micelles	Adsorption coefficient (1/wt %)	Packing fraction (%)	Fraction of adsorbed micelles (%)
HS40	16.0 ± 0.5	$2.1 \pm 0.2 \times 10^{15}$	0.125 ± 0.004	804 ± 50	0.38 ± 0.01	15 ± 1	5.20 ± 0.20	28 ± 3	44 ± 4
TM40	27.0 ± 0.8	$4.4 \pm 0.4 \times 10^{14}$	0.074 ± 0.002	2290 ± 135	0.22 ± 0.01	65 ± 3	7.35 ± 0.23	51 ± 5	35 ± 3

here, therefore, is only from that of the adsorbed micelles and/or free micelles. Both the data match in the higher-Q region where the scattering is contributed by both the adsorbed and free micelles. On the other hand, the buildup in the scattering data in the low-Q region is governed by the distribution of adsorbed micelles. The comparison of structure factor of adsorbed micelles on HS40 and TM40 nanoparticles is shown in Fig. 6(c). The structure factor is enhanced with a shift towards lower Q on increasing the size of the nanoparticles. The fitted parameters of particle size-dependent micelle adsorption on nanoparticles are given in Table I. It is found that the number of adsorbed micelles per nanoparticle and packing fraction increases significantly with the increase in the size of the nanoparticle which is also pointed out by the increase in the scattering intensity in the low-Q region for TM40 nanoparticles. This indicates that the nanoparticle curvature is definitely an important factor in determining the resultant adsorption of micelles on nanoparticles. However, the fraction of the adsorbed micelles decreases, which can be expected as the surface available to micelle adsorption decreases with the increase in the nanoparticle size (decrease in the surface-to-volume ratio). The micelles on nanoparticles do not pack in the close packing pattern possibly because the micelle adsorption is largely governed by micelle-nanoparticle interaction and not by micelle-micelle interaction. The micelle adsorbed on the nanoparticle surface (via hydrogen bonding) at a particular location may influence or restrict the position of the further adsorbed micelles. Such adsorption is completely random and thus does not lead to a close packing arrangement.

The scattering profiles of 1 wt % TM40 silica nanoparticles with varying concentration of C12E10 when nanoparticles are contrast-matched are shown in Fig. 7. Data show a rise in the scattering at the low- and mid-Q region with an increase in the surfactant concentration from 0.1 to 1 wt % as previously observed in the case of HS40. The enhancement in scattering in the low-Q region is definitely attributed to more and more surfactant micelles introduced in each step of an increase in concentration, and their subsequent adsorption on the nanoparticle surface. Unlike for HS40, the contribution of structure factor of adsorbed micelles in the scattering profiles for TM40 is distinct for all the C12E10 concentrations. In the low-Q region, the saturation of buildup of scattering is observed faster for TM40 than HS40. This can be attributed to the overall reduced availability of surface for adsorption due to the bigger size of TM40 silica nanoparticles. Evidence to support this can be found from DLS results of TM40 with varying concentration of C12E10 as shown in Fig. 8. The mean hydrodynamic size is observed to increase from 31 to 38 nm throughout the C12E10 concentration range. It is also observed that the variation in mean hydrodynamic size with respect to C12E10 concentration is similar in form for both TM40 and HS40 nanoparticles. The increase in hydrodynamic size for TM40 tends to saturate faster as compared to HS40.

The adsorption curves from SANS analysis for differently sized silica nanoparticles expressed as the number of

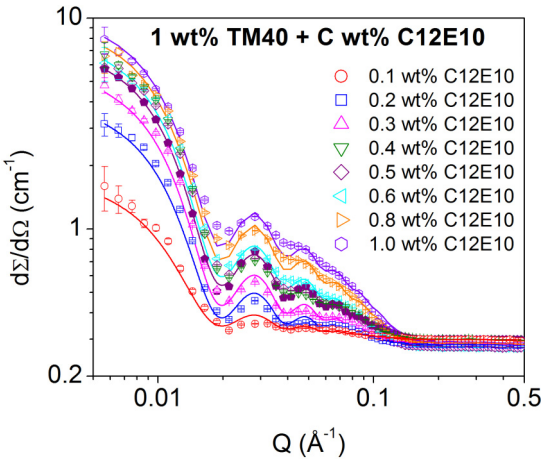

FIG. 7. SANS profiles for 1 wt % TM40 nanoparticle in presence of varying C12E10 surfactant concentration (0.1–1 wt %) with the condition of nanoparticles are contrast-matched.

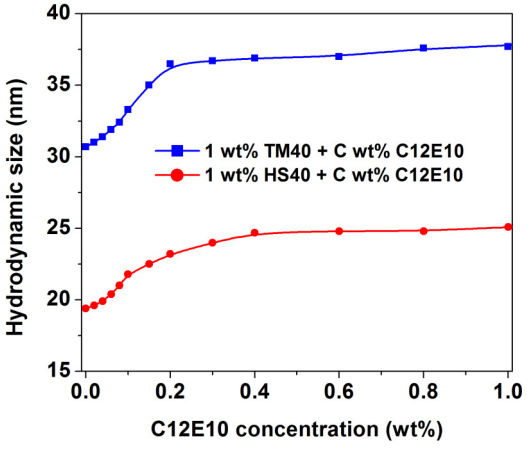

FIG. 8. The variation of mean hydrodynamic size in 1 wt % TM40 silica nanoparticles and comparison with 1 wt % HS40 silica nanoparticles as a function of C12E10 surfactant concentration over a range of (0–1 wt %).

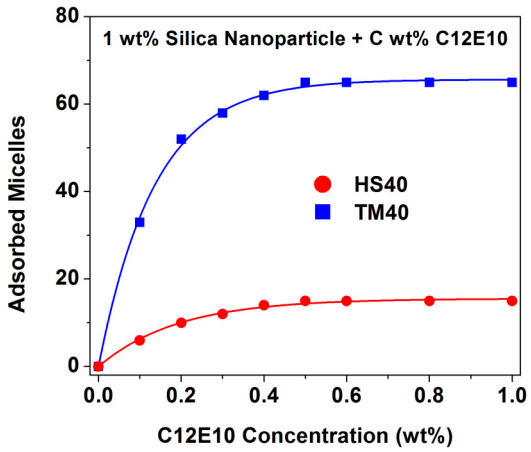

FIG. 9. Comparison of adsorption curves for C12E10 micelles interacting with differently sized HS40 and TM40 silica nanoparticles.

adsorbed micelles per nanoparticle with varying concentration of C12E10 are depicted in Fig. 9. Considering both these isotherms under the condition where the size of nanoparticles is distinctly different, one finds that the overall trend of the isotherm is similar for different adsorbent sizes. In both the curves, in the initial stages of the adsorption (the surfactant concentration is well below CMC), the surfactant is adsorbing on a surface where there are very few molecules and the adsorbate-adsorbate interaction is insignificant. With the introduction of more and more numbers of surfactant molecules, the formation of local monolayers (hemimicelles) and then local bilayers (micelles) begins. At higher surfactant concentrations, the slope of the adsorption curve proceeds towards saturation [27,59]. As it is understood that the average limit of the maximum number of adsorbed micelles on each nanoparticle decides the plateau of the adsorption curve, it is clear that the adsorption capability (in terms of the number of adsorbed micelles on each nanoparticle) is higher for TM40 than HS40. However, the fraction of the adsorbed micelles, an equally significant aspect, shows the opposite trend. The decrease in the fraction of adsorbed micelle with an increase in the size of the nanoparticle is attributed to the overall reduction in the available surface (surface area of one nanoparticle $\times$ number density of nanoparticles) for the micelle adsorption. For TM40, the larger particle will have a lower number density (for a fixed concentration) and hence the effective coverage of the nanoparticle surface will be attained with a lesser fraction of available micelles. The rate of attainment of a constant plateau region and the packing fraction of the micelles on the nanoparticle are also related to the surface curvature of the adsorbent. With the rise in the concentration

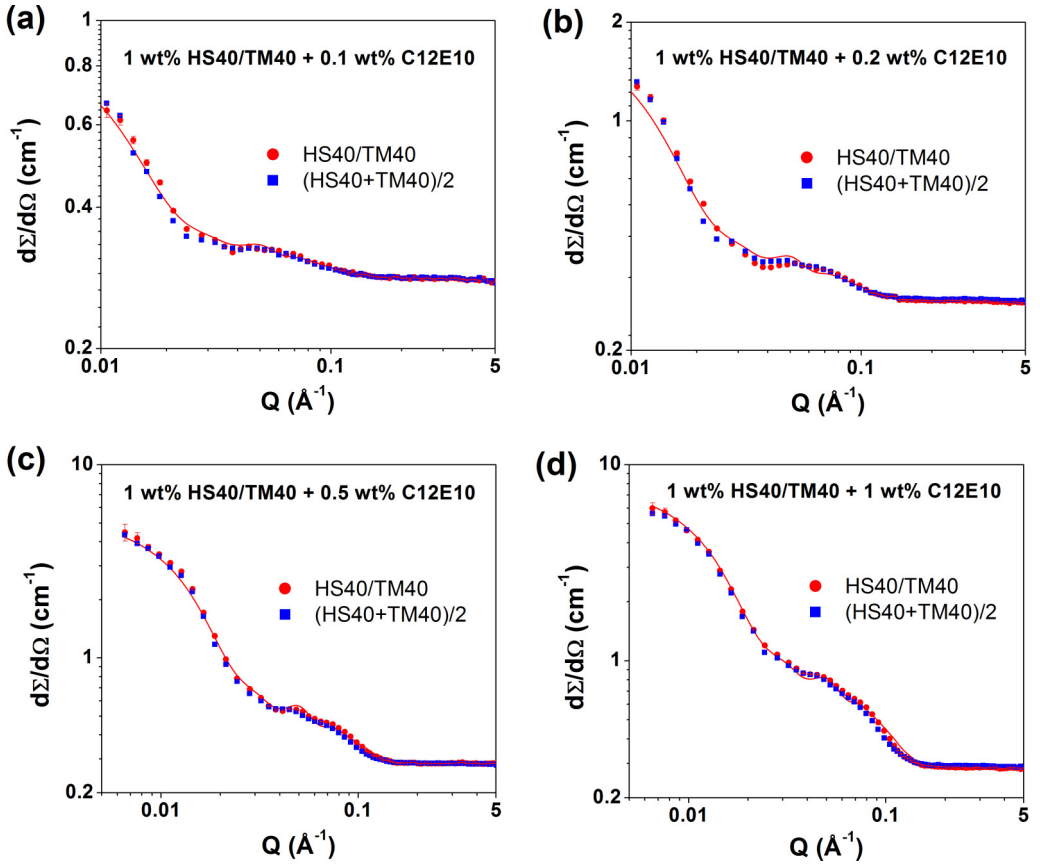

FIG. 10. SANS profiles for 1 wt % mixed nanoparticles (HS40/TM40) in presence of varying C12E10 surfactant concentration (0.1, 0.2, 0.5, and 1 wt %) with the condition of nanoparticles are contrast-matched (in 62 vol % D_2O). Averaged SANS data of pure nanoparticles (1 wt %) with corresponding C21E10 surfactant concentrations are also shown for comparison.

of micelles, the micelles supported on a high curvature experience different balances of *A*-*A* (amphiphile-amphiphile) and *A*-*S* (amphiphile-surface) interaction than that on flat curvature. The high surface curvature of the silica nanoparticles (HS40) prevents an effective packing of the hydrophobic tails of the molecules in a bilayer configuration. On the other hand, micelles on a low curvature surface (TM40) can have favorable *A*-*S* interactions without significant changes in aggregate structure, that is, without sacrificing the *A*-*A* interaction energy [27,38,51,60]. This evidently shows that the adsorption parameters derived from two different-sized nanoparticles are quite contrasting. Considering this, it creates a possibility that the adsorption of nonionic micelles on silica nanoparticles can be tuned through a bimodal size distribution of nanoparticles. Though the phenomenon of adsorption of surfactant on a single-sized nanoparticle surface has been inspected actively, there have been no studies with mixed systems involving differently sized nanoparticles. This aspect has been examined by the adsorption phenomenon for the mixed system of differently sized nanoparticles (HS40/TM40) in the presence of C12E10.

The SANS data of mixed 1 wt % HS40/TM40 silica nanoparticle system (0.5 wt % HS40 + 0.5 wt %TM40) interacting with varying concentration of C12E10 when nanoparticles are contrast-matched are shown in Fig. 10. If each concentration is specifically looked into, the scattering from the mixed HS40/TM40 system is somewhat higher than that from pure HS40 and lower than that from pure TM40. To investigate this, SANS data of a mixed 1 wt % HS40/TM40 (0.5 wt % HS40 + 0.5 wt % TM40) nanoparticle system have been compared to the mathematically averaged data of the individual scattering from their pure configurations (1 wt % HS40 and 1 wt %TM40) interacting with nonionic surfactant. Depending on the concentration of the surfactant and its subsequent adsorption (in different self-assembled conformations), the functionality is obviously different. However, the scattering profile of the mixed system of differently sized nanoparticles matches that of the averaged pure nanoparticles system in the presence of C12E10 for all the concentrations. It seems that surfactant distribution on the nanoparticle surface does not get affected in the presence of a combination of differently sized nanoparticles. The surfactant molecules self-assemble and similarly distribute themselves as they do for an individual nanoparticle and there is no size-dependent preferential adsorption in the case of the simultaneous presence of differently sized nanoparticles. The nonpreference of micelle adsorption for different-sized nanoparticles at higher surfactant concentrations can be easily understood when all the nanoparticles have been saturated. There is enough concentration of surfactant for the micelles to adsorb on all the nanoparticles. However, the nonpreference of micelle adsorption for different-sized nanoparticles at lower surfactant concentrations is quite interesting. This suggests that micelles get randomly distributed with equal probability irrespective of the size of the nanoparticles. These results can be used to systematically tune the adsorption behavior of micelles of nanoparticles by varying the concentration of one size in the mixed different-sized nanoparticles.

IV. CONCLUSIONS

SANS and DLS have been used to study the adsorption of nonionic surfactant C12E10 as a function of surfactant concentration for two different sizes of anionic silica nanoparticles. SANS measurements have been carried out under different contrast-matched conditions to simplify the analysis and probe the changes in both surfactant and nanoparticles in the complexes. The SANS data with contrast-matched nanoparticles reveal that the adsorption of nonionic surfactants on a nanoparticle results in the formation of micelle-adsorbed nanoparticles and the number of adsorbed micelles increases with increasing surfactant concentration. The adsorption follows an exponential behavior with increasing surfactant concentration. The packing fraction of adsorbed micelles strongly depends on nanoparticle curvature and increases with the nanoparticle size. The adsorption coefficient of the concentration dependent exponential behavior also increases with the increase in the nanoparticle size. On the other hand, the fraction of adsorbed micelles decreases with the increase in nanoparticle size because of a decrease in the surface-to-volume ratio. In the case of the number density of the silica nanoparticles with different sizes being the same, the fraction of the adsorbed micelles will be higher for the largest particles as both the low curvature (higher packing fraction) and high surface area (higher number of adsorbed micelles) support higher adsorption. In the mixed systems of different sizes of the nanoparticles, there is no preferential selectivity observed for the adsorption of micelles on nanoparticles, suggesting that the micelles are randomly distributed with equal probability on the nanoparticles.

ACKNOWLEDGMENTS

The neutron experiments at the Materials and Life Science Experimental Facility at J-PARC were approved by the neutron science program review committee (Proposal No. 2019B0033). This work was supported by a Grant-in-Aid for Scientific Research on Innovative Areas (Grant No. JP19H05717; Aquatic Functional Materials).

[1] A. C. Balazs, T. Emrick, and T. P. Russell, Science **314**, 1107 (2006).

[2] R.-L. Duan, X. Sun, J. Liu, T. Gong, and Z.-R. Zhang, Acta Pharmacol. Sin. **32**, 108 (2011).

[3] I. Yadav, S. Kumar, V. K. Aswal, and J. Kohlbrecher, Phys. Rev. E **89**, 032304 (2014).

[4] S. Rana, Y.-C. Yeh, and V. M. Rotello, Curr. Opin. Chem. Biol. **14**, 828 (2010).

[5] H. Heinz, C. Pramanik, O. Heinz, Y. Ding, R. K. Mishra, D. Marchon, R. J. Flatt, I. Estrela-Lopis, J. Llop, S. Moya, and R. F. Ziolo, Surf. Sci. Rep. **72**, 1 (2017).

[6] S. Palchetti, D. Pozzi, M. Mahmoudi, and G. Caracciolo, J. Mater. Chem. B **4**, 4376 (2016).

[7] C. Varea, R. A. Barrio, and A. Hernández-Machado, Phys. Rev. E **84**, 061922 (2011).

[8] J. Israelachvili, *Intermolecular and Surface Forces* (Academic, London, 2011).

[9] V. J. Anderson and H. N. W. Lekkerkerker, Nature (London) **416**, 811 (2002).

[10] J. A. Mysona, A. V. McCormick, and D. C. Morse, Phys. Rev. E **102**, 022605 (2020).

[11] M. E. Leunissen, C. G. Christova, A.-P. Hynninen, C. P. Royall, A. I. Campbell, A. Imhof, M. Dijkstra, R. van Roij, and A. van Blaaderen, Nature (London) **437**, 235 (2005).

[12] A. Sambasivam, A. V. Sangwai, and R. Sureshkumar, Langmuir **32**, 1214 (2016).

[13] I. Yadav, V. K. Aswal, and J. Kohlbrecher, Phys. Rev. E **91**, 052306 (2015).

[14] Z. Nie, A. Petukhova, and E. Kumacheva, Nat. Nanotechnol. **5**, 15 (2010).

[15] D. Maillard, S. K. Kumar, A. Rungta, B. C. Benicewicz, and R. E. Prud'homme, Nano Lett. **11**, 4569 (2011).

[16] F. Zhao and J. Xu, Colloid Polym. Sci. **285**, 113 (2006).

[17] D. Myers, *Surfactant Science and Technology* (Wiley, Hoboken, NJ, 2006).

[18] T. F. Tadros, *Applied Surfactants: Principles and Applications* (Wiley-VCH, Weinheim, 2005).

[19] S. Ahualli, G. R. Iglesias, W. Wachter, M. Dulle, D. Minami, and O. Glatter, Langmuir **27**, 9182 (2011).

[20] S. Kumar and V. K. Aswal, J. Phys.: Condens. Matter **23**, 035101 (2011).

[21] D. Ray and V. K. Aswal, J. Phys.: Condens. Matter **26**, 035102 (2014).

[22] D. Ray, V. K. Aswal, and J. Kohlbrecher, J. Appl. Phys. **117**, 164310 (2015).

[23] D. Ray, S. Kumar, V. K. Aswal, and J. Kohlbrecher, Langmuir **34**, 259 (2018).

[24] S. Partyka, S. Zaini, M. Lindheimer, and B. Brun, Colloids Surf. **12**, 255 (1984).

[25] F. Tiberg, J. Chem. Soc., Faraday Trans. **92**, 531 (1996).

[26] F. Tiberg, B. Joesson, and B. Lindman, Langmuir **10**, 3714 (1994).

[27] S. Paria and K. C. Khilar, Adv. Colloid Interface Sci. **110**, 75 (2004).

[28] S. M. Kirby, S. L. Anna, and L. M. Walker, Soft Matter **14**, 112 (2018).

[29] H. Ma, M. Luo, and L. L. Dai, Phys. Chem. Chem. Phys. **10**, 2207 (2008).

[30] A. K. Y. Raman and C. P. Aichele, Colloids Surf. A **585**, 124084 (2020).

[31] S. Takata, J. Suzuki, T. Shinohara, T. Oku, T. Tominaga, K. Ohishi, H. Iwase, T. Nakatani, Y. Inamura, T. Ito, K. Suzuya, K. Aizawa, M. Arai, T. Otomo, and M. Sugiyama, JPS Conf. Proc. **8**, 036020 (2015).

[32] D. Ray and V. K. Aswal, in *Solid State Physics: Proceedings of the 58th DAE Solid State Physics Symposium 2013*, AIP Conf. Proc. No. 1591, edited by C. Murli, D. Bhattacharyya, and S. C. Gadkari (AIP, Melville, NY, 2014), pp. 175–177.

[33] J. B. Hayter and J. Penfold, Mol. Phys. **42**, 109 (1981).

[34] E. W. Kaler, J. Appl. Crystallogr. **21**, 729 (1988).

[35] J. S. Pedersen, Adv. Colloid Interface Sci. **70**, 171 (1997).

[36] J. S. Pedersen, J. Appl. Crystallogr. **33**, 637 (2000).

[37] G. Despert and J. Oberdisse, Langmuir **19**, 7604 (2003).

[38] D. Lugo, J. Oberdisse, M. Karg, R. Schweins, and G. H. Findenegg, Soft Matter **5**, 2928 (2009).

[39] J. Teixeira, J. Appl. Crystallogr. **21**, 781 (1988).

[40] I. Bressler, J. Kohlbrecher, and A. F. Thünemann, J. Appl. Crystallogr. **48**, 1587 (2015).

[41] P. R. Bevington, *Data Reduction and Error Analysis for Physical Sciences* (McGraw-Hill, New York, 1969).

[42] R. Pecora, *Dynamic Light Scattering* (Plenum, New York, 1985).

[43] P. A. Hassan, S. Rana, and G. Verma, Langmuir **31**, 3 (2015).

[44] D. E. Koppel, J. Chem. Phys. **57**, 4814 (1972).

[45] P. Lindner and T. Zemb, in *Neutrons, X-rays and Light: Scattering Methods Applied to Soft Condensed Matter* (North-Holland, Amsterdam, 2002), pp. 203–220.

[46] E. Venugopal, V. K. Aswal, and G. Kumaraswamy, Langmuir **29**, 9643 (2013).

[47] J. Oberdisse, Phys. Chem. Chem. Phys. **6**, 1557 (2004).

[48] B. Bharti, *Adsorption, Aggregation and Structure Formation in Systems of Charged Particles* (Springer, Cham, 2014).

[49] P. G. Cummins, J. Penfold, and E. Staples, J. Phys. Chem. **96**, 8092 (1992).

[50] J. Penfold, E. Staples, I. Tucker, and P. Cummins, J. Phys. Chem. **100**, 18133 (1996).

[51] D. M. Lugo, J. Oberdisse, A. Lapp, and G. H. Findenegg, J. Phys. Chem. B **114**, 4183 (2010).

[52] K. P. Sharma, V. K. Aswal, and G. Kumaraswamy, J. Phys. Chem. B **114**, 10986 (2010).

[53] J. E. Fieldsend and R. M. Everson, *Multiobjective Problem Solving from Nature. Natural Computing Series* (Springer, Heidelberg, 2008).

[54] S. Kumar, V. K. Aswal, and J. Kohlbrecher, Langmuir **27**, 10167 (2011).

[55] S. Kumar, I. Yadav, V. K. Aswal, and J. Kohlbrecher, Langmuir **34**, 5679 (2018).

[56] S. J. Clunie and B. T. Ingram, in *Adsorption from Solution at the Solid/Liquid Interface*, edited by G. D. Parfitt and C. H. Rochester (Academic, New York, 1983), Chap. 3, pp. 97–171.

[57] J. M. Corkill, J. F. Goodman, and J. R. Tate, Trans. Faraday Soc. **62**, 979 (1966).

[58] R. Denoyel and J. Rouquerol, J. Colloid Interface Sci. **143**, 555 (1991).

[59] B. Bharti, J. Meissner, U. Gasser, and G. H. Findenegg, Soft Matter **8**, 6573 (2012).

[60] I. Yadav, V. K. Aswal, and J. Kohlbrecher, Phys. Rev. E **93**, 052601 (2016).